Rational design of a fluorescent NADPH derivative imaging constitutive nitric-oxide synthases upon two-photon excitation.

Yun Li, Huan Wang, Bogdan Tarus, Miguel Romero Perez, Laurence Morellato, Etienne Henry, Vladimir Berka, Ah-Lim Tsai, Booma Ramassamy, Hamid Dhimane, et al.

Rational design of a fluorescent NADPH derivative imaging constitutive nitric-oxide synthases upon two-photon excitation

Yun Li[a,1], Huan Wang[b,1], Bogdan Tarus[c,1], Miguel Romero Perez[d], Laurence Morellato[a], Etienne Henry[b], Vladimir Berka[e], Ah-Lim Tsai[e], Booma Ramassamy[a], Hamid Dhimane[a], Chantal Dessy[d], Patrick Tauc[b], Jean-Luc Boucher[a], Eric Deprez[b,1,2], and Anny Slama-Schwok[c,1,2]

[a]Laboratoire de Chimie et Biochimie Pharmacologiques et Toxicologiques, Centre National de la Recherche Scientifique UMR8601, Université Paris Descartes, 75270 Paris, France; [b]Laboratoire de Biologie et Pharmacologie Appliquée, Centre National de la Recherche Scientifique UMR8113, ENS-Cachan, 94235 Cachan, France; [c]Laboratoire de Virologie et Immunologie Moléculaires, Institut National de la Recherche Agronomique UR892, 78350 Jouy en Josas, France; [d]Pole of Pharmacology and Therapeutics, FATH5349, Institute of Experimental and Clinical Research, Université catholique de Louvain Medical Sector, B-1200 Brussels, Belgium; and [e]Division of Hematology, Department of Internal Medicine, University of Texas Health Science Center at Houston, TX 77030

Edited by* Gregory A. Petsko, Brandeis University, Waltham, MA, and approved June 25, 2012 (received for review April 3, 2012)

We report the structure-based design and synthesis of a unique NOS inhibitor, called nanoshutter NS1, with two-photon absorption properties. NS1 targets the NADPH site of NOS by a nucleotide moiety mimicking NADPH linked to a conjugated push–pull chromophore with nonlinear absorption properties. Because NS1 could not provide reducing equivalents to the protein and competed with NADPH binding, it efficiently inhibited NOS catalysis. NS1 became fluorescent once bound to NOS with an excellent signal-to-noise ratio because of two-photon excitation avoiding interference from the flavin–autofluorescence and because free NS1 was not fluorescent in aqueous solutions. NS1 fluorescence enhancement was selective for constitutive NOS in vitro, in particular for endothelial NOS (eNOS). Molecular dynamics simulations suggested that two variable residues among NOS isoforms induced differences in binding of NS1 and in local solvation around NS1 nitro group, consistent with changes of NS1 fluorescence yield. NS1 colocalized with eNOS in living human umbilical vein endothelial cells. Thus, NS1 constitutes a unique class of eNOS probe with two-photon excitation in the 800–950-nm range, with great perspectives for eNOS imaging in living tissues.

chemical biology | inhibition of enzymatic catalysis | structure-based design and molecular modeling | two-photon fluorescence imaging | fluorescence spectroscopy

In mammals, NO is a gaseous signaling mediator that exerts a wide range of key physiological functions, including blood pressure regulation, neurotransmission, and immune responses (1). NO is formed by nitric-oxide synthases, a family of hemoproteins that catalyzes the oxidation of L-arginine leading to L-citrulline and NO (2, 3). NOS catalysis is driven by reducing equivalents supplied by NADPH. NOS enzymes are constituted by oxygenase and reductase domains linked by a calmodulin (CaM)-binding domain. The oxygenase domain binds the heme, L-arginine, and the cofactor (6*R*)-5,6,7,8-tetrahydro-L-biopterin (H_4B). The reductase domain binds two flavins, FMN and FAD, and NADPH (4). CaM binding allows the electron transfer from FMN to the heme (2, 3). The biological activities of NO are closely linked to the specific NOS isoform involved in its synthesis and deregulation of its biosynthesis leads to various pathologies (5). Data support the notion that inhibition of the inducible and neuronal isoforms iNOS and nNOS have therapeutic utility in the treatment of a variety of diseases, including septic shock, neurodegeneration, inflammation, and cancer (5, 6). It was shown that the endothelial isoform eNOS participates in tumor initiation and maintenance, thus its inhibition could be beneficial in this context (7, 8). Based on crystallographic studies (9, 10), much effort was dedicated to the development of specific NOS inhibitors by targeting the heme site. However, most of these inhibitors are not specific and cannot avoid NOS uncoupling and formation of deleterious radical oxygen species (ROS) at the reductase domain. Although the structure of nNOS reductase domain has been solved (4), no specific compounds targeting this domain are available, and only diphenyliodonium (DPI) and its analogs nonselectively and irreversibly react with flavins (11). The NADPH-binding site is highly conserved among redox enzymes. The crystallographic data of NADPH-containing proteins showed that the main recognition elements in their binding site involve conserved arginines that interact electrostatically with the 2′ phosphate group of NADPH nucleotide moiety. The nicotinamide part of NADPH can be flexible and undergoes conformational changes depending on the NADP(H) enzymes and their specific catalysis. In recent studies, we have characterized a NADPH analog called nanotrigger, NT1, targeting the NADPH site in NOS reductase domain (12–14) (Fig. 1*A*). NT1 contained a conjugated, photoactivatable chromophore substituted with two donor groups that replaced the nicotinamide moiety of NADPH. Following photoactivation, the terminal amine group of excited NT1* was able to inject electrons to the FAD acceptor, thereby initiating the electron flow. This initiation and synchronization of NOS catalysis upon one- or two-photon excitation (1-PE or 2-PE, respectively) led to light-induced NO formation (12–14).

Here, we designed a unique prototype of NOS inhibitor, called nanoshutter (NS1), with intrinsic fluorescence imaging properties. To this purpose, we designed a compound that meets the following criteria: (*i*) NS1 should demonstrate a good affinity for NOS, at least comparable to the affinity of the natural hydride donor NADPH; (*ii*) injection of electrons to FAD should be prohibited by bound NS1 to NOS; (*iii*) NS1 should have a good two-photon cross-section, compatible with multiphoton imaging; (*iv*) free and bound NS1 should possess different fluorescence properties. We designed a compound bearing a nucleotide moiety as recognition motif of the NADPH site linked by an alkyl chain to a new chromophore substituted with an acceptor and a donor group, thus engineering a push–pull photoactive element

Author contributions: Y.L., J-L.B., C.D., E.D., and A.S.-S. designed research; Y.L., H.W., B.T., M.R.P., L.M., E.H., V.B., and P.T. performed research; B.T., V.B, A.-L.T., P.T., and J.-L.B. analyzed data; and E.D. and A.S.-S. wrote the paper.

The authors declare no conflict of interest.

*This Direct Submission article had a prearranged editor.

[1]Y.L., H.W., B.T., E.D. and A.S.-S. contributed equally to this work.

[2]To whom correspondence may be addressed. E-mail: Anny.Schwok@gmail.com or deprez@lbpa.ens-cachan.fr.

This article contains supporting information online at www.pnas.org/lookup/suppl/doi:10.1073/pnas.1205645109/-/DCSupplemental.

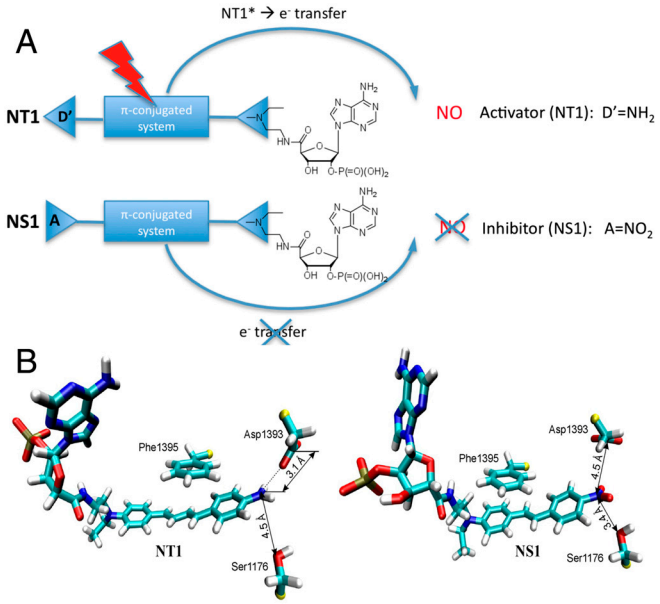

Fig. 1. Design and molecular modelling studies of the nanotrigger NT1 and the nanoshutter NS1. (*A*) Principles of activation and inhibition of NOS by NT1 and NS1. Because of its terminal nitro-phenyl (electron acceptor) group that cannot inject the reducing equivalents required for the initiation of catalysis, NS1 is expected both to bind to the NADPH site and to inhibit competitively the electron flow to the FAD acceptor (in contrast to the electron donor–containing compound NT1). Additionally, significant modulations of the fluorescence emission by the polarity (λ_{max}) and the presence of water (quantum yield, Φ) of the environment are expected. (*B*) Close-up view of the terminal groups of NT1 diene chromophore and NS1stilbene chromophore in $nNOS_{red}$; FAD is omitted for clarity (12–14).

(Fig. 1*A*). Such a chomophore is expected to have a high dipole moment caused by the electron delocalization in the excited state that should lead to nonlinear absorption properties (15). The NS1 chromophore carries a conjugated stilbene substituted with the donor–acceptor pair instead of the diene moiety of NT1 (13) (Fig. 1*B*). Finally, the terminal electron acceptor was chosen to be a nitro group that should block the electron flow, inhibit NOS catalysis, and modulate the fluorescence properties of NS1 with the environment (16). A change in fluorescence emission between free and NOS-bound states of the engineered NS1 compound was then expected. This work paves the way for a unique family of NOS inhibitors with imaging applications.

Results

Molecular Modelling. We showed that NS1 fits into the narrow NADPH site of the reductase domain of nNOS ($nNOS_{red}$) using docking and molecular dynamic simulations based on the structure of this domain (4). We used a stilbene moiety instead of the 1,4-diphenyl-butadiene moiety of NT1 for replacement of the nicotinamide part of NADPH. This choice of a shorter stilbene moiety was guided by initial modelling studies, which had suggested that a shorter compound than NT1 with the same terminal donor group could fit tighter to this site. Our design retained the nucleotidic recognition motif of NADPH that confers proper targeting to the NADPH site, based on previous studies that led to the discovery of NT1 (12–14, 17). The designed inhibitor NS1 was docked in $nNOS_{red}$ by replacement of the embedded NADPH (4). Each complex, NS1-$nNOS_{red}$ or NT1-$nNOS_{red}$, was placed in a box of explicit water molecules; after energy minimization, we assessed the fit of both NS1 and NT1 within the NADPH site by running trajectories of 10 ns. The main interaction energy of NS1 and NT1 with the protein originated in their terminal phosphate group that recognized the conserved arginine residues in the NADPH-binding site, in particular Arg1400, Arg1314, Arg1284, and Arg1010. This modelling demonstrated a similar recognition of the nucleotidic part of NS1 to that seen with NADPH (17) (*SI Appendix*, Fig. S1 and Table S1). The chromophore moieties of NS1 and NT1 were inserted close to FAD, removing the stacking interaction of Phe1395 with FAD observed in the crystal structure (4). The partly charged oxygen of the terminal nitro group of NS1 induced a reorientation of the δ-oxygen of Asp1393 by electrostatic repulsion between them (Fig. 1*B*). The van der Waals energy terms of both chromophores had similar negative values, contributing to their correct docking despite unfavorable electrostatic energies, 25 ± 5 and 9 ± 4 kcal/mol for NS1 and NT1, respectively. The better steric fit of the stilbene chromophore to the NADPH site was reflected by a more favourable linker term for NS1 binding than for NT1 (-57 ± 6 and -38 ± 7 kcal/mol, respectively) (*SI Appendix*, Table S1). In NT1, the positioning of the longer diene chromophore probably required some adjustments. Altogether, the nucleotidic part was identical in both molecules and there was compensation between the linker and chromophore energy terms, which led to similar interaction energies for both NS1 and NT1, suggesting that NS1 could display an affinity for nNOS (or eNOS) close to that of NT1.

Synthesis, Spectroscopic, and Fluorescence Properties of NS1 in Solution. The synthesis of the target compound NS1 (Fig. 2*A*) consisted of a seven-step procedure (see *Methods* and *SI Appendix*, Fig. S2). The absorption spectra of NS1 and its chromophore

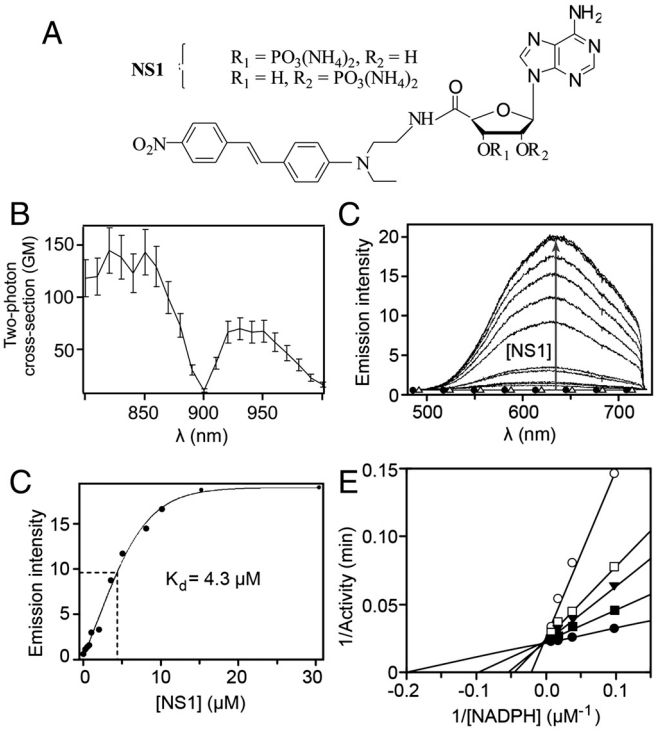

Fig. 2. Binding of NS1 to nNOS monitored by fluorescence emission upon 2-PE and subsequent inhibition of NOS activity. (*A*) Structure of NS1; (*B*) two-photon excitation spectrum of NS1 in DMSO. The fluorescence quantum yield and the two-photon cross-section (σ_2) were determined using rhodamine B as a reference and were found to be equal to 0.0045 and 65 GM at 940 nm, respectively (σ_2 of approximately 130 GM at 840 nm). (*C*) Increase in NS1 fluorescence ($\lambda_{ex,\,2\text{-PE}} = 940$ nm) upon binding to nNOS (5 μM). No fluorescence emission was detected in Tris buffer upon 2-PE of nNOS alone (△) or NS1 alone (30 μM, ●); (*D*) corresponding binding isotherm. The binding isotherm was fitted using a one-binding site model, leading to an apparent dissociation constant for NS1 binding of 4.3 ± 0.6 μM. (*C*) Inhibition by NS1 of the formation of NO by nNOS: competition experiments between NADPH and NS1. The double-reciprocal plots of nNOS activities measured in the presence of various concentrations of NADPH (up to 100 μM) are shown in the absence (●) or in the presence of 5 (■), 25 (▼), 50 (□), or 100 (○) μM NS1.

moiety were similar, with a maximum similar to the related 4-*N,N*-dimethylamino-4′-nitrostilbene (16, 18). NS1 had an absorption maximum at $\lambda_{max} = 460$ nm with an extinction coefficient $\varepsilon = 21{,}000\ M^{-1}\,cm^{-1}$ in DMSO (*SI Appendix*, Fig. S3*A*); upon excitation at 460 nm, NS1 presented a broad emission peak centred at 740 nm (*SI Appendix*, Fig. S3*B*). The two-photon cross-section of NS1 was found to be σ_2 of approximately 130 and 65 GM (Göppert-Mayer; 1 GM = 10^{-50} cm^4·s/photon) in the 800–860 and 920–950 nm ranges, respectively, in DMSO (Fig. 2*B*). As expected, NS1 fluorescence was strongly sensitive to the presence of water (*SI Appendix*, Fig. S3 *B* and *C*), its fluorescence was undetectable in aqueous solutions under either one-photon excitation condition (at 435 or 460 nm) or two-photon excitation condition ($\lambda_{ex,2\text{-PE}} = 840$ or 940 nm).

Fluorescence Properties of NS1–NOS Complexes. Addition of NS1 to purified NOS led to the recovery of bound NS1 fluorescence as compared to free NS1 being non fluorescent in aqueous buffer. This made possible the biochemical monitoring of NS1 binding to NOS using one- or two-photon fluorescence experiments. Under 1-PE conditions, the intrinsic emission properties of the NS1–nNOS complex were difficult to extract because the fluorescence of nNOS flavins and the fluorescence of NS1 overlapped. NS1 contribution was extracted by monitoring the emission at 700 nm in a spectral region where flavin autofluorescence was not significant. Although NS1 fluorescence was low at 700 nm, NS1 binding to nNOS could be recorded and led to the determination of an apparent K_d of 4.2 μM (*SI Appendix*, Fig. S4). We reasoned that if the two-photon fluorescence of nNOS is weak (as expected, taking into account the very low σ_2 value of flavins—see *Discussion*), the 2-PE approach should be more appropriate for monitoring the fluorescence recovery of NS1 upon binding to nNOS. Indeed, both the intrinsic fluorescence of nNOS and free NS1 fluorescence (up to 30 μM) were undetectable under 2-PE condition (Fig. 2*C*). Stepwise additions of NS1 to nNOS resulted in an increase of NS1 fluorescence emission (Fig. 2*C*), which corresponded to pure emission spectra of NS1 in the nNOS–NS1 complex, allowing quantitative analysis of the binding process (Fig. 2*D*). The apparent $K_d = 4.3 \pm 0.6$ μM was consistent with the 1-PE value. The emission of NS1 was blue-shifted in the protein context (630 nm) compared to DMSO (740 nm), consistent with the influence of solvent polarity on emission maxima of nitrostilbene derivatives (16). Binding of NS1 to full-length eNOS, iNOS, or $eNOS_{red}$ yielded comparable results in terms of affinity, but with substantial differences in the quantum yield characterizing each complex (see below).

Inhibition of NOS Catalytic Activity by NS1. The ability of NS1 to inhibit the NADPH-mediated hydride transfer to nNOS was studied by stopped-flow measurements. Fast mixing of nNOS with NADPH resulted in a fast decrease of the NADPH absorption, corresponding to a two-phase model (*SI Appendix*, Fig. S5). A significant slowdown of the fast phase of NADPH consumption that contributed approximately 65% of the decay at 340 nm was observed in the presence of NS1. NS1 competed with NADPH on nNOS reduction in a dose-dependent manner, presenting a typical saturation curve, and led to an apparent inhibition constant $K_i = 15 \pm 4$ μM. This value compares well with those obtained previously with NT1, $K_i = 7 \pm 3$ μM (13, 17), showing that NS1 and NT1 display similar affinities for the NADPH site of constitutive NOS, as suggested by our molecular modelling study.

Because NS1 abolished the electron-transfer flux from NADPH to the flavins in the reductase domain of nNOS, NO formation should also be inhibited. The ability of NS1 to inhibit NO formation was assessed using the oxyhemoglobin assay. NS1 inhibited the formation of NO catalyzed by nNOS in a dose-dependent manner with a half-inhibitory concentration (IC_{50}) at 65 ± 8 μM in the presence of 100 μM NADPH and L-arginine (*SI Appendix*, Fig. S6*A*). We then investigated the mechanism of inhibition by varying NADPH and NS1 concentrations. The double-reciprocal plot of NO formation activity as a function of [NADPH] led to a K_m value of 5.5 ± 0.5 μM in the absence of NS1 (intercept with the *x* axis; Fig. 2*E*). NS1 inhibition was competitive with NADPH as demonstrated by changes of the apparent K_m values ($K_{m\,app}$) without significant effect on the V_{max} values with varying NS1 concentration. The plot of $K_{m\,app}$ values as a function of [NS1] led to a K_i value ranging between 13 and 18 μM (*SI Appendix*, Fig. S6*B*). The value of $K_i = 3.4$ μM deduced from $IC_{50} = 65$ μM using the Cheng-Prusoff relationship is consistent with the values of $K_d = 4.3$ μM and $K_i = 15$ μM obtained in 2-PE and stopped-flow experiments, respectively, and compares well with NADPH affinity ($K_m = 5.5 \pm 0.5$ μM). Further experiments using the dilution method showed that the inhibition of NO formation by NS1 was reversible. NS1 appears as a unique prototype inhibitor that competes with NADPH for binding in the reductase domain.

In Vitro Selectivity in the Fluorescence Enhancement of Protein-Bound NS1. The relative two-photon fluorescence intensity of NS1 bound to various proteins was next assessed. NS1 did not display significant fluorescence enhancement in the presence of proteins lacking a NADPH-binding site (Fig. 3*A*). For instance, NS1 nonspecifically binding to the fatty acid–binding protein (FABP) accounted for only 5% of the fluorescence signal observed with eNOS-bound NS1. Thus, NS1 differs from nonspecific probes such as the well-known ANS compound (anilinonaphthalene sulfonic acid), whose fluorescence is largely enhanced by multiple interactions in inner protein cavities, in particular upon binding to FABP (19). Among the NADPH-binding proteins, including the three NOS isoforms, NS1 binding to eNOS and nNOS led to the largest fluorescence enhancement (eNOS > nNOS ≫ iNOS). The fluorescence quantum yield of NS1 was found to be strongly dependent on the protein context, indicating that NS1 within the NADPH-binding site probed distinct local solvent environment in each NOS isoform. In contrast, NS1 was only weakly fluorescent when bound to ferredoxin reductase or glucose-6-phosphate dehydrogenase (G6PDH). Interestingly, the two-photon fluorescence emission of eNOS-bound NS1 was found to be even higher than the value found in DMSO (approximately 45-fold higher) (Fig. 3*A*, *Inset*). Thus, NS1 is highly selective between constitutive and inducible NOS. These results were promising for further cellular investigations.

Structural Insight of NS1 Binding to NOS Isoforms Based on Molecular Dynamics Simulations. We attempted to explain the modulation in fluorescence yields of NS1 bound to the three NOS isoforms by additional structural insight; homology modelling was used to generate eNOS and iNOS reductase domains (17). NS1 bound to nNOS or eNOS by three arginine residues interacting with its phosphate group (*SI Appendix*, Fig. S7). Among these arginines, R1400 in nNOS was replaced in iNOS by S1130 unable to form an H-bond with NS1 phosphate. Note that S1130 is located on the same linker as the catalytic D1123, allowing an information flow between the nucleotidic part of NS1 and the chromophore terminal. In addition, the solvation around NS1 terminal NO_2 was highest in iNOS among the three NOS (*SI Appendix* and Fig. 3 *B* and *C*) and *SI Appendix* (Fig. S8). The importance of water in active sites of proteins has been shown by pioneer works of Douzou and co-workers (20). In iNOS, the NO_2 group of the chromophore was more distant to the hydrophobic patch forming the edge of the binding site. This patch was composed by three F and one Y in iNOS and nNOS instead of four F in eNOS. Y1077 made H-bonds with either water or nearby hydrophilic residues, which caused the hydrophobic patch to be less packed, and more water (partly from iNOS dimeric interface) accessed the NO_2 group (*SI Appendix*, Fig. S8). In contrast,

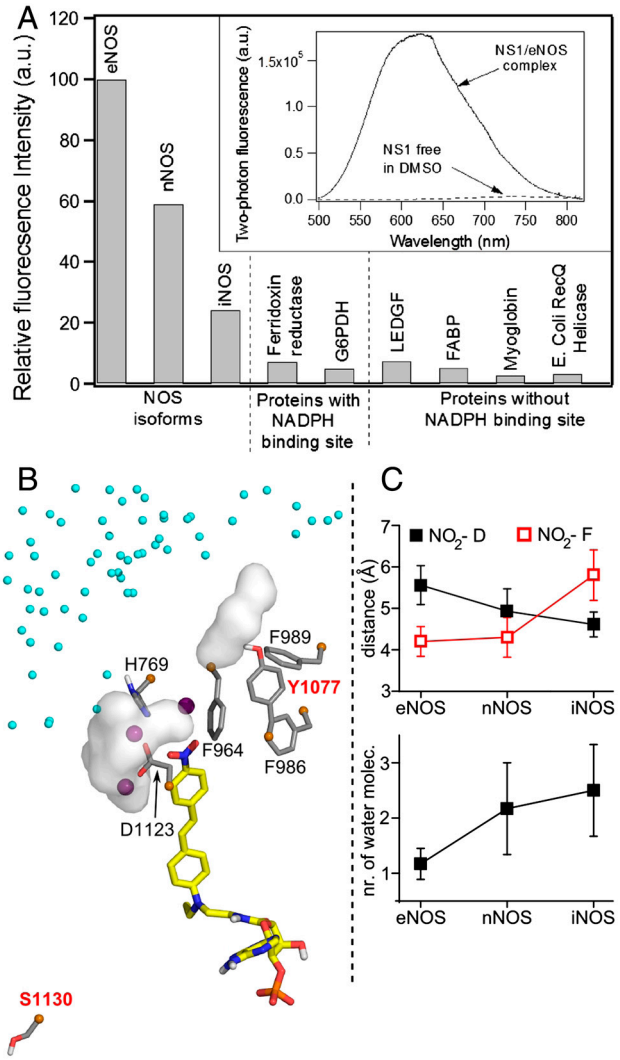

Fig. 3. (*A*) Fluorescence intensity of NS1 bound to various proteins upon two-photon excitation (normalized by the maximum intensity value corresponding to eNOS). The experiments shown in Fig. 2*C* and *D* were repeated with NOS isoforms and proteins with ferredoxin reductase, glucose-6-phosphate dehydrogenase (G6PDH), or without [lens epithelium–derived growth factor (LEDGF), fatty acid–binding protein (FABP), myoglobin, and *E. Coli* RecQ helicase] a NADPH-binding site; 5 μM of protein was mixed with increasing concentrations of NS1 until the fluorescence intensity reached a plateau. The relative fluorescence intensity was calculated based on the plateau value. The apparent dissociation constants of NS1 from the NOS isoforms determined using 2-PE fluorescence display similar affinities for NS1, $K_d = 4$–5 μM. (*Inset*) Two-photon fluorescence emission of NS1 (ex 940 nm) bound to eNOS or free in DMSO. (*B*) Zoom on the solvation near the nitro terminal of NS1 chromophore bound to iNOS reductase domain. Three water molecules located at 3.5 Å from the NO_2 extremity of NS1 are shown by purple spheres. The white surfaces are solvent molecules at 3.5 Å from D1123 and (variable) Y1077, the latter being part with F986, F989, and F964 to the hydrophobic patch at the edge of NS1-binding site; contribution of water from iNOS dimeric interface (small cyan spheres) is observed; (*C*) The distance to the conserved *D* decreases while the distance to F (F998, F1234, F964) and the number of water surrounding D (D1157, D1393, D1123) increases in the order e/n/iNOS (*SI Appendix*, Fig. S8).

the proximity of NO_2 to a well-packed hydrophobic patch limited access to water-solvating D1127 in eNOS; thus, NS1 terminal probed a more hydrophobic environment. This hypothesis fits well with NS1's probing the most hydrophobic environment in eNOS, thus the largest fluorescent yield. Indeed, specific solvent effects depending on the water content modulate NS1 fluorescence yield without $\lambda_{max,em}$ shift in solution and in NOS isoforms (*SI Appendix*, Fig. S3 and Fig. 3*A*).

NS1 Imaging in Endothelial Cells. The fluorescence selectivity of NS1 for constitutive NOS prompted us to test if NS1 would specifically highlight eNOS in living cells. A rapid uptake of NS1 (maximum 10 min) by living human umbilical vein endothelial cells (HUVECs) was easily monitored upon excitation in the near infrared, showing the suitability of NS1 for 2-PE fluorescence studies of living cells (Fig. 4). (A comparison between 1- and 2-PE images for identical living cells is shown in *SI Appendix*, Fig. S9). NS1 displayed an intense fluorescence signal in the cytoplasm, especially in the perinuclear region and, to a smaller extent, at the cell membrane (Figs. 4*A* and 5 *A* and *D*). The dots at the cell membranes were prominent at high cell confluence, in agreement with the role of eNOS in the maintenance of tight cell-to-cell junctions (21). The subcellular localization of NS1 within organelles was then further investigated by colocalization experiments. NS1 mainly colocalized with the Golgi apparatus (Fig. 4 *E*–*H*). NS1 did not colocalize with the endoplasmic reticulum, cell nucleus, or mitochondria, whereas only partial colocalization was observed with early endosome (EEA1) (*SI Appendix*, Fig. S10). The two main locations of NS1 (Golgi and plasma membrane) are compatible with the subcellular localization of eNOS (22). Using specific immunostaining of eNOS combined to one- (Fig. 5 *A*–*C*) or two-photon (Fig. 5 *D*–*F*) imaging of NS1, we observed an excellent colocalization of NS1 and eNOS in the perinuclear region and at the plasma membrane level, showing that NS1 actually targets eNOS in HUVEC cells. Because the 2-PE process avoided cellular autofluorescence, the signal-to-noise ratio was remarkably higher using two-photon compared to one-photon imaging, as judged by the more restricted colocalization area obtained using $\lambda_{ex} = 840$ nm instead of 488 nm.

Discussion

NS1 fulfilled a double functionality: (*i*) a new prototype of a reversible NOS inhibitor, targeting the reductase domain in a specific manner and competing with NADPH; (*ii*) a unique fluorescent compound with 2-PE properties when bound to constitutive eNOS or nNOS. These two functions result from a rational design of a push–pull nitroaminostilbene chromophore moiety that cannot inject reducing equivalents required for triggering NOS catalysis, and that is highly sensitive to solvent polarity and to the presence of water in terms of fluorescence quantum yield (16).

Available NOS inhibitors include analogs of substrate L-arginine, calmodulin antagonists, and irreversible flavin inhibitor DPI and its analogs (11) as nonspecific inhibitors of electron transfer. NS1 represents a unique prototype of NOS inhibitor that competes with the initial hydride donor NADPH for binding to the reductase domain. Consequently, NS1 appears as a site-specific, reversible inhibitor that prevents both NO formation and NOS uncoupling by blocking the electron flow (flavins and heme). As such, avoiding the formation of toxic ROS and NO concentrations offers great perspectives, in particular for therapeutic strategies for, on the one hand, targeting nNOS and iNOS in the treatment of neurodegeneration, inflammation, and cancer (5), and, on the other hand, controlling eNOS activity and inhibiting deleterious effects of NO produced by eNOS in metastasis (7). Because eNOS constitutes the major source of NO production in endothelial cells and is an important regulator of cardiovascular homeostasis, further work is in progress for improving the isoform selectivity of NS1 in terms of molecular recognition, as well as for developing a photoactivation strategy for spatial and temporal control of eNOS inhibition by a two-photon–induced process.

In terms of NS1 imaging, a specific fluorescence enhancement upon binding to constitutive NOS was observed, with a preference for eNOS over nNOS. Compared to available NOS ligands,

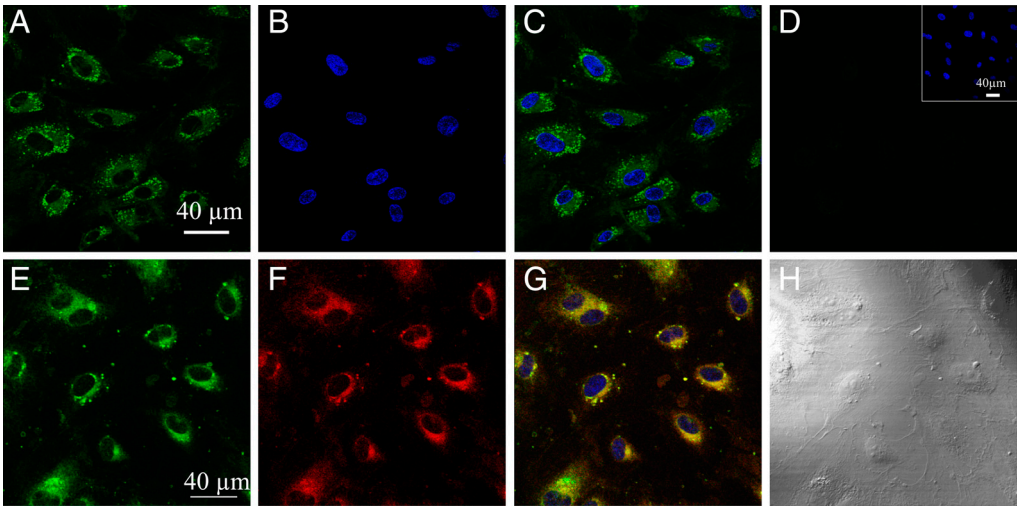

Fig. 4. Imaging of living HUVECs using the two-photon fluorescence properties of NS1 and colocalization with the Golgi complex. HUVECs were treated with 5 μM NS1 and further observed under 2-PE (840 nm; emission at 520–680 nm) (*A*); (*B*) nucleus staining of NS1-treated HUVECs (2-PE, 740 nm; emission at 410–510 nm) by Hoechst 33342; (*C*) merged image of *A* and *B*; (*D*) control two-photon image of nontreated HUVECs at the same setting (*Inset*, nucleus staining of control cells); (*E–H*) colocalization imaging of NS1 and the Golgi complex—living HUVECs were treated with NS1 (5 μM) and Golgi tracker (BODIPY TR ceramide; 5 μM) for 60 min. (*E*) Shows the imaging channel of NS1 (1-PE, 488 nm; emission at 520–680 nm). (*F*) Shows the imaging channel of the Golgi tracker (1-PE, 543 nm; emission at 600–650 nm); (*G*) merged image of *E* and *F* (with nucleus staining). Yellow areas indicate colocalization of NS1 and the Golgi apparatus; (*H*) shows the corresponding differential interference contrast microscopy transmission image. Colocalization experiments with ER, mitochondria, and EEA1 are shown in *SI Appendix*, Fig. S10.

NS1 has the additional benefit of real-time imaging eNOS in living endothelial cells with excellent signal-to-noise ratio. This is of special interest because confinement effects on the subcellular location of eNOS have a profound effect on eNOS activity and are altered in pathological states (23). NS1 was highly photostable, without fading or blinking compared to fluorescent proteins (FP) or quantum dots (QD), respectively, and probed endogenous expression profiles of eNOS in contrast to exogenous fusion or QD-labeled proteins. Moreover, NS1 internalization did not require permeation mandated for immunostaining when using antibodies against eNOS. The excellent signal-to-noise ratio primarily relies on NS1 fluorescence enhancement by binding to eNOS with negligible fluorescence either free or with nonspecific proteins. Additionally, NS1 is well-suited for two-photon studies because it has a much higher two-photon cross-section ($\sigma_2 = 130$ and 65 GM at 840 and 940 nm, respectively) than that of flavins and NAD(P)H (24, 25) [σ_2 (flavins) $= 0.8$ and 0.1 GM at 700 and 900 nm, respectively, or σ_2 (NADPH) $= 5 \cdot 10^{-2}$ and $5 \cdot 10^{-6}$ GM at 700 and 900 nm, respectively]. Thus, the intrinsic advantage of NS1 relies on its two-photon absorption properties and ability for monitoring native eNOS using 2-PE without background or free NS1 contribution.

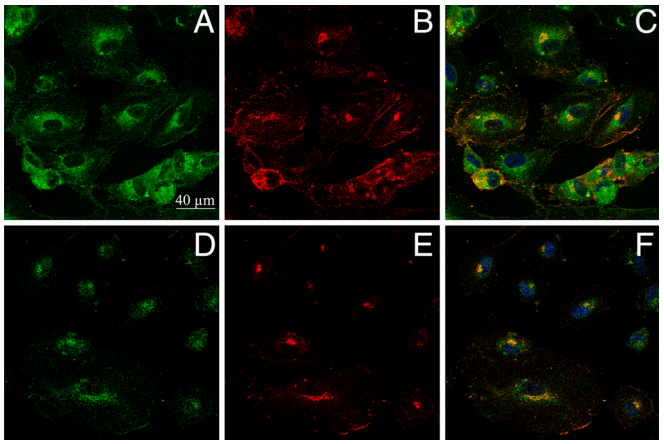

Fig. 5. Colocalization imaging of NS1 and eNOS. Living HUVECs were treated with NS1 (10 μM) for 60 min prior to fixation and immunostaining of eNOS. Primary and secondary antibodies for immunostaining were purified mouse anti-eNOS/NOS Type III and AlexaFluor 594 goat anti-mouse IgG (H + L), respectively. (*A* and *D*) Imaging channel of NS1 [1-PE (488 nm) and 2-PE (840 nm), respectively; emission at 520–680 nm]; (*B* and *E*) imaging channel of eNOS (1-PE, 543 nm; emission at 590–700 nm), corresponding to *A* and *D*, respectively; (*C*) merged image of *A* and *B*; (*F*) merged image of *D* and *E*. Yellow to orange areas indicate colocalization of NS1 and eNOS. Nucleus staining by Hoechst 3342 is also shown in *C* and *F*. Upon prolonged incubations (1–3 h) with NS1 (1–10 μM), the cells did not modify their shapes without fading of NS1signal upon 1-PE and 2-PE.

In conclusion, NS1 is a promising tool for noninvasive imaging of living tissues and isolated organs with an enhanced spatial resolution and a better light penetration in living tissues, leading to potential applications for monitoring eNOS within tumor cells as melanoma. Improvement of the selectivity of the NS1 prototype toward nNOS should afford an interesting pharmacological and imaging tool for neurodegenerative diseases.

Methods

Molecular Modelling. Molecular dynamics simulations of nNOS–NS1 and nNOS–NT1 complexes were carried out using the program NAMD with the CHARMM27 force field (26). eNOS and iNOS reductase domains were generated by homology modelling based on the structure of the nNOS isoform (1TLL) (4). The solvent was treated explicitly. Electrostatic interactions were calculated with no truncation, using the particle mesh Ewald summation algorithm. The van der Waals interactions were smoothly shifted to zero between 10.0 Å and 12.0 Å. The list of the nonbonded interactions was truncated at 13.5 Å. The lengths of the bonds containing hydrogen atoms were fixed with the SHAKE algorithm, allowing us to use an integration time of 2 fs. Trajectories of 10 ns each were produced for nNOS-bound NS1 and NT1 and for the eNOS–NS1 and iNOS–NS1complexes.

Synthesis of NS1. The substituted aldehyde **3** was prepared from *N*-ethylaniline and phthalimido-acetaldehyde **1** in the presence of $NaBH(OAc)_3$, followed by a Vilsmeier formylation of disubstituted aniline **2**. The Knoevenagel-type condensation of 4-nitrophenyl-acetic acid with **3** led to the pure *E*-4-(4-nitrostyryl)aniline derivative **4**. The phthalimido group was removed using the $NaBH_4$-HOAc method (27). A peptide coupling reaction with HBTU in anhydrous DMF assembled the chromophore **5** and the 2′-3′-*iso*-propylidene adenosine 5-carboxylic acid **6** (28). After HCl deprotection of the *iso*-propylidene moiety of compound **7**, diol **8** was phosphorylated at positions 2′ and 3′ by treatment with chlorodiethylphosphate in anhydrous CH_2Cl_2. Further acidic hydrolysis of the diethylphosphate afforded the

expected NS1 as a mixture of isomeric compounds **9** and **10** bearing the $P(O)(OH)_2$ group at positions 2′ and 3′ in a 40:60 ratio, respectively (see *SI Appendix*, Fig. S2).

Expression and Purification of Proteins. Recombinant rat nNOS, murine iNOS, and bovine eNOS were expressed in *Escherichia coli* BL21 cells whereas eNOS reductase domain was expressed in yeast and purified as described (29, 30).

Spectroscopic Characterization of Free or NOS-Bound NS1. UV-visible absorption spectrum of NS1 was carried out with an Uvikon spectrophotometer. Fluorescence excitation and emission spectra under one-photon excitation condition were recorded on an Eclipse (Varian) fluorimeter. Two-photon excitation and emission spectra were recorded using a home-built setup. Briefly, an 80-MHz mode-locked Mai-Tai Ti:Sapphire tunable laser (690–1,040 nm, 100-fs laser pulse; Spectra Physics) was focused onto the sample placed in a quartz micro cell. The fluorescence was collected at 90°, filtered by a Semrock FF01-842/SP filter, and focused into an optical fiber connected to a SpectraPro-275 digital spectrograph coupled to CCD detector (Princeton Instruments).

Stopped-Flow Experiments. Kinetics of the reaction between nNOS (5 μM) and NADPH were measured at 24 °C in an anaerobic chamber (Coy Laboratory Products Inc.) using a Bio-SEQUENTIAL DX-18MV stopped-flow instrument (Applied Photophysics). The solutions of NADPH (25 μM) and NS1 (0–100 μM) were prepared in oxygen-free buffer. Reaction rates were calculated by fitting data to single- or double-exponential functions using Applied Photophysics software.

Effect of NS1 on the Formation of NO Catalyzed by nNOS. The initial rates of NO formation were determined at 37 °C in 1-cm path-length cuvettes (150 μl) on a Uvikon 941 spectrophotometer using the oxyhemoglobin assay. The NO-mediated conversion of oxyhemoglobin to methemoglobin was monitored by repetitive scanning between 380 and 480 nm every 0.2 min. All values are means ± SD from 3–4 experiments.

Imaging of Living HUVEC Cells in the Presence of NS1 and Colocalization Experiments. NS1 was incubated with HUVECs (Sigma, at fourth passage) for 30 min using fresh medium before observation. One- and 2-photon images of living NS1-treated HUVECs were obtained using a SP2 confocal microscope (Leica MicroSystems) and a laser line at 488 nm or an 80-MHz mode-locked Mai-Tai Ti:Sapphire laser (720–920 nm, 100-fs laser pulse; Spectra Physics) tuned to 840 nm, respectively (the emission range was set between 520 and 680 nm). Colocalization experiments of NS1 with endoplasmic reticulum (ER), mitochondria, or Golgi complex were performed on living HUVEC cells using ER-Tracker Red dye, MitoTracker Deep Red FM, or BODIPY TR ceramide complexed to BSA (Invitrogen), respectively. Colocalization of NS1 with early endosome (EEA1) or eNOS was performed by immunostaining on fixed cells using rabbit polyclonal to EEA1 marker (Abcam) or purified mouse anti-eNOS/NOS Type III (BD-Biosciences), respectively, as primary antibodies.

ACKNOWLEDGMENTS. The authors thank Dr. Lambry for providing initial parameter files and Dr. Lee-Ho Wang (University of Texas Health Science Center at Houston, TX) for providing protein samples. This work was funded by the French National Research Agency Grant (ANR-PCVI08-006-01 to A.S.-S., J.-L.B., and E.D.) and fellowships (to B.T. and L.M.) and National Institutes of Health Grant HL095820 (to A.-L.T.). This work was granted access to the High Performance Computing (HPC) resources of Institut du Développement et des Ressources en Informatique Scientifique (IDRIS) made by Grand Equipement National de Calcul Intensif (GENCI) under Grant 2010-99636 (to A.S.-S. and B.T.).

1. Moncada S, Palmer RM, Higgs EA (1991) Nitric oxide: Physiology, pathophysiology and pharmacology. *Pharmacol Rev* 43:109–142.
2. Jachymova M, et al. (2005) Recruitment of governing elements for electron transfer in the nitric oxide family. *Proc Natl Acad Sci USA* 102:15833–15838.
3. Li H, Poulos TL (2005) Structure-function studies on nitric oxide synthases. *J Inorg Biochem* 99:293–305.
4. Garcin ED, et al. (2004) Structural basis for isozyme-specific regulation of electron transfer in nitric-oxide synthase. *J Biol Chem* 279:37918–37927.
5. Pacher P, Beckman JS, Liaudet L (2007) Nitric oxide and peroxynitrite in health and disease. *Physiol Rev* 87:315–424.
6. Silverman RB (2009) Design of selective neuronal nitric oxide synthase inhibitors for the prevention and treatment of neurodegenerative diseases. *Acc Chem Res* 42:439–451.
7. Lim KH, Ancrile BB, Kashatus DF, Counter CM (2008) Tumour maintenance is mediated by eNOS. *Nature* 452:646–649.
8. Lahdenranta J, et al. (2009) Endothelial nitric oxide synthase mediates lymphangiogenesis and lymphatic metastasis. *Cancer Res* 69:2801–2808.
9. Crane BR, et al. (2000) Structures of the N(omega)-hydroxy-L-arginine complex of inducible nitric oxide synthase oxygenase dimer with active and inactive pterins. *Biochemistry* 39:4608–4621.
10. Raman CS, et al. (1998) Crystal structure of constitutive endothelial nitric oxide synthase: A paradigm for pterin function involving a novel metal center. *Cell* 95:939–950.
11. Stuehr DJ, et al. (1991) Inhibition of macrophage and endothelial cell nitric oxide synthase by diphenyleneiodonium and its analogs. *FASEB J* 5:98–103.
12. Beaumont E, et al. (2009) NO formation by neuronal NO-synthase can be controlled by ultrafast electron injection from a nanotrigger. *Chembiochem* 10:690–701.
13. Beaumont E, et al. (2007) Synchronous photoinitiation of endothelial NO synthase activity by a nanotrigger targeted at its NADPH site. *J Am Chem Soc* 129:2178–2186.
14. Beaumont E, et al. (2008) Two photon-induced electron injection from a nanotrigger in native endothelial NO-synthase. *ChemPhysChem* 9:2325–2331.
15. Akemann W, Laage D, Plaza P, Martin MM, Blanchard-Desce M (2008) Photoinduced intramolecular charge transfer in push–pull polyenes: Effects of solvation, electron-donor group, and polyenic chain length. *J Phys Chem B* 112:358–368.
16. Lapouyade R, Kuhn A, Letard JF, Rettig W (1993) Multiple relaxation pathways in photoexcited dimethylaminonitro- and dimethylaminocyano-stilbenes. *Chem Phys Lett* 208:48–58.
17. Lambry JC, Beaumont E, Tarus B, Blanchard-Desce M, Slama-Schwok A (2010) Selective probing of a NADPH site controlled light-induced enzymatic catalysis. *J Mol Recognit* 23:379–388.
18. Paper V, Pines D, Likhenstein G, Pines E (1997) Photophysical characterization of trans-4,4′- disubstituted stilbenes. *J Photochem Photobiol A* 111:87–96.
19. Kirk WR (2005) The binding of 1,8 ANS congeners to I-FABP and comparison of some hypotheses about ANS' spectral sensitivity to environment. *Biochim Biophys Acta* 1748:84–93.
20. Di Primo C, Deprez E, Hoa GH, Douzou P (1995) Antagonistic effects of hydrostatic pressure and osmotic pressure on cytochrome P-450cam spin transition. *Biophys J* 68:2056–2061.
21. Rath G, Dessy C, Feron O (2009) Caveolae, caveolin and control of vascular tone: Nitric oxide (NO) and endothelium derived hyperpolarizing factor (EDHF) regulation. *J Physiol Pharmacol* 60(Suppl 4):105–109.
22. Fulton D, et al. (2002) Localization of endothelial nitric-oxide synthase phosphorylated on serine 1179 and nitric oxide in Golgi and plasma membrane defines the existence of two pools of active enzyme. *J Biol Chem* 277:4277–4284.
23. Villanueva C, Giulivi C (2010) Subcellular and cellular locations of nitric oxide synthase isoforms as determinants of health and disease. *Free Radic Biol Med* 49:307–316.
24. Huang S, Heikal AA, Webb WW (2002) Two-photon fluorescence spectroscopy and microscopy of NAD(P)H and flavoprotein. *Biophys J* 82:2811–2825.
25. Xu HN, Nioka S, Glickson JD, Chance B, Li LZ (2010) Quantitative mitochondrial redox imaging of breast cancer metastatic potential. *J Biomed Opt* 15:036010.
26. Folloppe N, MacKerell AD (2000) All-atom empirical force field for nucleic acids: I. Parameter optimization based on small molecule and condensed phase macromolecular target data. *J Comp Chem* 21:86–104.
27. Benkeser RA, Laugal JA, Rappa A (1984) Safe method for reduction of aromatic compounds. *Terahedron Lett* 25:2089–2092.
28. Robin AC, et al. (2007) A NADPH substitute for selective photo-initiation of reductive bioprocesses via two-photon induced electron transfer. *Chem Comm* 43:13333–13336.
29. Moali C, Boucher JL, Sari MA, Stuehr DJ, Mansuy D (1998) Substrate specificity of NO synthases: Detailed comparison of L-arginine, homo-L-arginine, their *N* omega-hydroxy derivatives, and *N* omega-hydroxynor-L-arginine. *Biochemistry* 37:10453–10460.
30. Du M, Yeh HC, Berka V, Wang LH, Tsai AL (2003) Redox properties of human endothelial nitric-oxide synthase oxygenase and reductase domains purified from yeast expression system. *J Biol Chem* 278:6002–6011.